














Cite this: DOI: 10.1039/d3dt03010e

Silver(I) complexes containing antifungal azoles: significant improvement of the anti-*Candida* potential of the azole drug after its coordination to the silver(I) ion†

Mia Stanković, ^a Jakob Kljun, ^b Nevena Lj. Stevanović, ^a Jelena Lazic, ^c Sanja Skaro Bogojevic, ^c Sandra Vojnovic, ^c Matija Zlatar, ^d Jasmina Nikodinovic-Runic, ^c Iztok Turel, ^{*b} Miloš I. Djuran ^{*e} and Biljana Đ. Glišić ^{*a}

Inspired by the emergence of resistance to currently available antifungal therapy and by the great potential of metal complexes for the treatment of various diseases, we synthesized three new silver(I) complexes containing clinically used antifungal azoles as ligands, [Ag(ecz)₂]SbF₆ (**1**, ecz is econazole), {[Ag(vcz)₂]SbF₆}_n (**2**, vcz is voriconazole), and [Ag(ctz)₂]SbF₆ (**3**, ctz is clotrimazole), and investigated their antimicrobial properties. The synthesized complexes were characterized by mass spectrometry, IR, UV-vis and ¹H NMR spectroscopy, cyclic voltammetry, and single-crystal X-ray diffraction analysis. In the mononuclear complexes **1** and **3** with ecz and ctz, respectively, the silver(I) ion has the expected linear geometry, in which the azoles are monodentately coordinated to this metal center through the N3 imidazole nitrogen atom. In contrast, the vcz-containing complex **2** has a polymeric structure in the solid state in which the silver(I) ions are coordinated by four nitrogen atoms in a distorted tetrahedral geometry. DFT calculations were done to predict the most favorable structures of the studied complexes in DMSO solution. All the studied silver(I) complexes have shown excellent antifungal and good to moderate antibacterial activities with minimal inhibitory concentration (MIC) values in the ranges of 0.01–27.1 and 2.61–47.9 μM on the selected panel of fungi and bacteria, respectively. Importantly, the complexes **1–3** have exhibited a significantly improved antifungal activity compared to the free azoles, with the most pronounced effect observed in the case of complex **2** compared to the parent vcz against *Candida glabrata* with an increase of activity by five orders of magnitude. Moreover, the silver(I)-azole complexes **2** and **3** significantly inhibited the formation of *C. albicans* hyphae and biofilms at the subinhibitory concentration of 50% MIC. To investigate the impact of the complex **3** more thoroughly on *Candida* pathogenesis, its effect on the adherence of *C. albicans* to A549 cells (human adenocarcinoma alveolar basal epithelial cells), as an initial step of the invasion of host cells, was studied.

Received 14th September 2023,
Accepted 4th December 2023

DOI: 10.1039/d3dt03010e

rs.c.li/dalton

^aUniversity of Kragujevac, Faculty of Science, Department of Chemistry, R. Domanovića 12, 34000 Kragujevac, Serbia. E-mail: biljana.glisic@pmf.kg.ac.rs

^bUniversity of Ljubljana, Faculty of Chemistry and Chemical Technology, Večna pot 113, SI-1000 Ljubljana, Slovenia. E-mail: Iztok.Turel@fkt.uni-lj.si

^cUniversity of Belgrade, Institute of Molecular Genetics and Genetic Engineering, Vojvode Stepe 444a, 11042 Belgrade, Serbia

^dUniversity of Belgrade-Institute of Chemistry, Technology and Metallurgy, Department of Chemistry, Njegoševa 12, 11000 Belgrade, Serbia

^eSerbian Academy of Sciences and Arts, Knez Mihailova 35, 11000 Belgrade, Serbia. E-mail: milos.djuran@pmf.kg.ac.rs

† Electronic supplementary information (ESI) available: Fig. S1–S12 and Tables S1–S3. CCDC 2277941–2277943. For ESI and crystallographic data in CIF or other electronic format see DOI: <https://doi.org/10.1039/d3dt03010e>

Introduction

Fungal infections are a worldwide global health problem, affecting millions of patients per year. Many fungal species are responsible for these invasive infections, which kill about one and a half million people every year. These high mortality rates, which can exceed 50%, have been attributed to the difficulty of diagnosis, and shortcomings in the current antifungal arsenal.^{1–3} More than 90% of all reported fungal-related deaths result from species that belong to one of the four genera: *Cryptococcus*, *Candida*, *Aspergillus*, and *Pneumocystis*, although diseases caused by rarer fungi are becoming more common.⁴ Furthermore, it has been anticipated that global warming will bring new fungal diseases to mammals.⁵



Although fungi were recognized as pathogens prior to bacteria, progress in the development of effective antifungals has lagged in antibacterial research. The reason for this lies in the fact that the eukaryotic nature of fungi makes them metabolically and physiologically similar to mammalian cells, and therefore offers limited pathogen-specific targets.⁶ The key to the successful development of antifungal agents is based on their specificity to arrest or kill pathogenic fungal cells in preference to host cells. The variance between fungal and host cells, as well as the variance among different fungal cells, provide the basis for the identification of druggable targets for new antifungal agents.

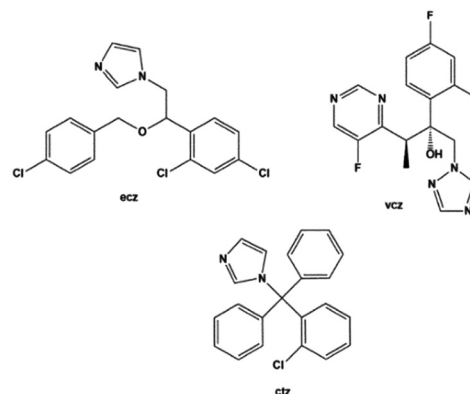
Up to now, only five main antifungal agent classes have been approved for human consumption: azoles, polyenes, echinocandins, allylamines, and antimetabolites.² The antifungal azoles are a principal class of small molecules that consist of an imidazole or a triazole ring attached to a carbon atom. They are used to treat fungal infections by targeting the cytochrome P450-dependent enzyme, sterol 14 α -demethylase (P450_{DM}), preventing the synthesis of ergosterol, a major component of fungal plasma membranes.⁷ However, the main drawbacks of currently used antifungal azoles include fungistatic rather than fungicidal activity, narrow spectrum of antifungal activity, non-optimal pharmacokinetics, and hepatotoxicity.⁸ Also, a common and serious problem of these, but also other, antifungal agents is the emergence of severe drug resistance, which has significantly reduced their therapeutic efficacy.^{9–13} The limited efficacy of azoles in the treatment of invasive fungal infections highlights the urgent need for the development of new agents, particularly new structures that act upon novel targets or that could overcome currently used antifungal drug side effects.

Metal ions can play an important role in modifying the pharmacological properties of known organic-based drugs, most of which can be coordinated with a metal ion. The resulting coordination compounds have different physical and pharmacological properties, and their mechanism of activity fundamentally differs from those of clinically used organic drugs. This can be explained by the fact that metal complexes of such organic drugs can have different geometries and generally possess a higher 3D character,^{14,15} which is one of the crucial factors in determining the biological activity of metal-based compounds.^{16–18} It is thus not surprising that research of metal complexes as antifungals is quite popular nowadays.^{19,20}

In light of the abovementioned facts, the complexation reactions between clinically used antifungal azoles and different metal ions (ruthenium(II), copper(II), zinc(II), silver(I) and gold(III)) have been recently investigated in our laboratories.^{21–24} The antimicrobial potential of metal-azole complexes obtained from these reactions was investigated by comparing their antimicrobial activity with that of the corresponding antifungal azoles. For instance, nine organoruthenium complexes with clotrimazole, tioconazole and miconazole have been evaluated against the fungus *Culvularia lunata*, showing significant antifungal activity, which decreased with the increasing number of

ligands.²¹ Further, the complexation reaction of fluconazole (fcz) with copper(II) and zinc(II) ions led to the formation of polymeric $\{[\text{CuCl}_2(\text{fcz})_2] \cdot 5\text{H}_2\text{O}\}_n$ and $\{[\text{ZnCl}_2(\text{fcz})_2] \cdot 2\text{C}_2\text{H}_5\text{OH}\}_n$ complexes of octahedral geometry, which have shown higher *in vitro* antifungal activity against *C. krusei* and *C. parapsilosis* than fluconazole.²² Moreover, these two complexes have shown strong inhibition of *C. albicans* filamentation and biofilm formation at subinhibitory concentrations. A high binding affinity of silver(I) ion for itraconazole (icz) was observed in the reaction between AgNO₃ and this antifungal drug. The spectroscopic and crystallographic results for the $[\text{Ag}(\text{icz})_2]\text{NO}_3 \cdot \text{H}_2\text{O}$ complex revealed that two icz ligands are monodentately coordinated to the silver(I) ion *via* the triazole nitrogen atom forming a cationic $[\text{Ag}(\text{icz})_2]^+$ part, which is neutralized by the nitrate anion.²³ The investigated silver(I) complex showed enhanced *in vitro* antifungal activity than icz, being 2.3- and 4.5-fold more active against *C. albicans* and *C. glabrata*, respectively. This complex was also more efficient in inhibiting yeast to hyphae transition process in *C. albicans*, as an important step in its pathogenesis. The toxicity evaluation in the zebrafish model (*Danio rerio*) suggests that the $[\text{Ag}(\text{icz})_2]\text{NO}_3 \cdot \text{H}_2\text{O}$ complex has a better therapeutic profile and improved antifungal efficacy with respect to the parent drug. More recently, the complexation reactions of four antifungal azoles (clotrimazole, econazole, tioconazole and voriconazole) with gold(III) ion have been performed, leading to the formation of the mononuclear gold(III) complexes of the general formula $[\text{AuCl}_3(\text{azole})]$.²⁴ These complexes demonstrated enhanced antimicrobial effectiveness than the corresponding azoles in most cases, with the best improvement obtained after the auration of tioconazole and voriconazole.

In the course of the above investigations, inspired by the differences in both potency and selectivity between the different antifungal azoles, herein we report the synthesis and structural characterization of new silver(I) complexes with clinically used antifungal azoles, econazole (ecz), voriconazole (vcz) and clotrimazole (ctz) (Scheme 1), namely $[\text{Ag}(\text{ecz})_2]\text{SbF}_6$ (1), $\{[\text{Ag}(\text{vcz})_2]\text{SbF}_6\}_n$ (2) and $[\text{Ag}(\text{ctz})_2]\text{SbF}_6$ (3). These complexes



Scheme 1 Structural formula of the antifungal azoles, econazole (ecz), clotrimazole (ctz) and voriconazole (vcz), used as ligands for the synthesis of silver(I) complexes in the present study.



along with the azoles used for their synthesis were evaluated for their *in vitro* antimicrobial activity against the panel of bacterial and *Candida* species, while their cytotoxicity was tested against the human normal lung fibroblast cell line (MRC-5). Moreover, the influence of complexes 2 and 3 on the formation of *C. albicans* hyphae and biofilms was studied at subinhibitory concentrations. The adherence of *C. albicans* to A549 cells (human adenocarcinoma alveolar basal epithelial cells) was investigated in the presence of the complex 3 to study its effect on *Candida* pathogenesis more thoroughly.

Results and discussion

Synthesis and structural characterization of the silver(I) complexes 1–3

Silver(I) complexes with the antifungal agents econazole (ecz), voriconazole (vcz) and clotrimazole (ctz), $[\text{Ag}(\text{ecz})_2]\text{SbF}_6$ (**1**), $\{\text{Ag}(\text{vcz})_2\}\text{SbF}_6\}_n$ (**2**) and $[\text{Ag}(\text{ctz})_2]\text{SbF}_6$ (**3**), were synthesized according to the procedure described in the Experimental section (*vide infra*). Silver(I) hexafluoroantimonate(V) was mixed with an equimolar amount of the corresponding azole in ethanol at ambient temperature. The crystals of the silver(I) complex **1** suitable for single-crystal X-ray diffraction analysis were obtained after the white precipitate from the reaction was recrystallized in acetonitrile, while the crystals of **2** and **3** were formed by recrystallization of the resulting precipitates in acetonitrile/ethanol (*v/v* 1/1) at ambient temperature. The composition of the synthesized complexes was elucidated from ^1H NMR, IR, UV-vis and mass spectra, elemental analysis measurement, DFT calculations and single-crystal X-ray diffraction analysis.

Crystal structure description and analysis. The structural aspect of metal complexes of azoles is quite poorly studied. The structural database CSD²⁵ (Cambridge Structural Database; WebCSD accessed on 16.10.2023) contains only one crystal structure of an econazole complex (gold(III) complex previously reported by our group),²⁴ 10 voriconazole complexes (4 Cu, 3 Ag, and 1 for Cd, Co, and Au) and 21 clotrimazole

complexes (6 Cu, 5 Ru, 3 Zn, 2 Au, and 1 for Pt, Pd, Rh, Mn, and Cd). Besides that, very recently, the crystal structure of *fac*-tricarbonylrhenium(I) complex bearing two different ligands, monodentate clotrimazole and bidentate 2,2'-bipyridine, has been reported.²⁶ Complexes **1** and **3** show relatively simple structures, both containing two monodentately N3-coordinated azole ligands (econazole and clotrimazole, respectively) forming a complex cation with linear geometry as expected (Fig. 1). The coordination mode of these azoles was the same at that of itraconazole (icz) previously observed in its silver(I) complex, $[\text{Ag}(\text{icz})_2]\text{NO}_3 \cdot \text{H}_2\text{O}$,²³ although Ag–N(ecz) and Ag–N(ctz) bond lengths of 2.089(4) and 2.090(3) Å, respectively, are slightly shorter than Ag–N(icz) bond lengths of 2.124(2) and 2.140(2) Å. In the structure of **3**, residual electron density was observed at approximately 1.6 Å from carbon atom C14 which corresponds to a possible $\text{C}_{\text{Ar}}\text{--Cl}$ distance. Thus, the chlorine atom was modelled to be disordered over carbon atoms C8 and C14 in a 92%/8%.

On the other hand, voriconazole as a ligand offers much greater potential for structural diversity because its structure includes four aromatic nitrogen atoms and an alcohol oxygen atom with coordination ability. The CSD²⁵ reports three known structures of silver(I)-vcz complexes synthesized with different salts as silver(I) source, namely, triflate, nitrate and perchlorate.^{27,28} We report here the crystal structure of a fourth complex containing hexafluoroantimonate(V) counter-anion (Fig. 2). These four structures can be divided into two groups. In the structure of **2**, vcz ligands bind to silver(I) in a 1 : 2 metal : ligand ratio. We can observe the same coordination pattern as in the triflate²⁸ and perchlorate²⁷ salts, which form polymeric structures in which silver(I) ions are coordinated by four nitrogen atoms and adopt a distorted tetrahedral geometry (Fig. 2). However, the two ligands are crystallographically different – molecule A acts as a terminal ligand, binding to only one Ag(I) ion through its N4A triazole nitrogen, and molecule B acts as a bridging ligand binding to three different silver(I) ions through the N1B and N4B triazole nitrogen atoms and the N14B pyrimidine nitrogen atom (Fig. 2). Each silver(I) ion is thus coordinated by four vcz ligand molecules. The pre-

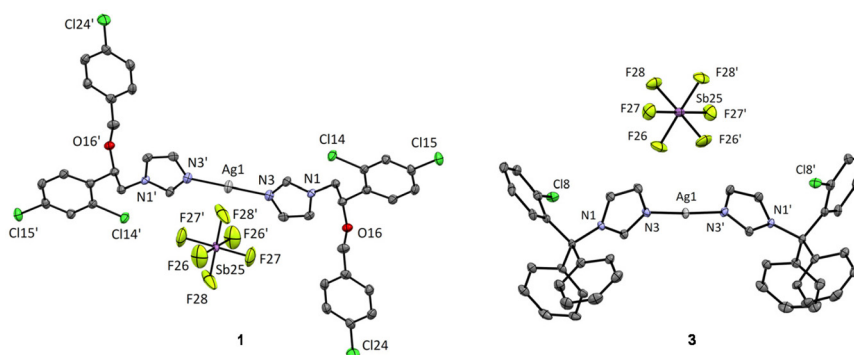


Fig. 1 Crystal structures of complexes **1** and **3** with heteroatom labelling. Thermal ellipsoids are shown at a 35% probability level. Hydrogen atoms are omitted. Chlorine atom C18 disorder in **3** is also omitted. Selected bond lengths and angles: (**1**) Ag1–N3 2.089(4) Å, N3–Ag1–N3' 180°, (**3**) Ag1–N3 2.090(3) Å, N3–Ag1–N3' 177.3°.



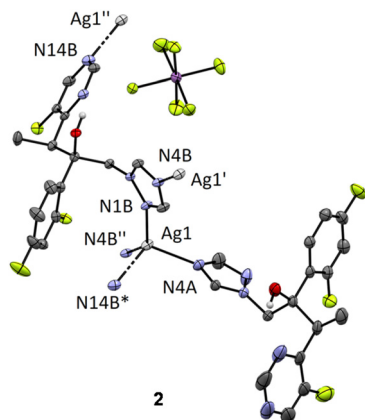


Fig. 2 Crystal structure of complex **2** with selected heteroatom labeling. Thermal ellipsoids are shown at 35% probability level. Hydrogen atoms are omitted. Selected bond lengths and angles: (2) Ag1–N1B 2.252(5) Å, Ag1–N14B 2.463(5) Å, Ag1–N4A 2.273(5) Å, Ag1–N4B 2.243(5) Å, N1B–Ag1–N14B 97.84(19)°, N1B–Ag1–N4A 107.2(2)°, N4A–Ag1–N14B 106.49(19)°, N4B–Ag1–N1B 137.46(19)°, N4B–Ag1–N14B 97.76(17)°, N4B–Ag1–N4A 105.76(19)°.

viously reported silver(I)-vcz complex with nitrate counter-anion, on the other hand, has a much more cross-linked structure in which we can observe that the asymmetric unit contains two different silver(I) ions (one tetracoordinated and one pentacoordinated) and four bridging ligands.²⁷

Spectroscopic characterization. The IR spectra of silver(I) complexes **1–3** in the wavenumber range of 4000–450 cm⁻¹ are in accordance with their structures determined by single-crystal X-ray diffraction analysis. These spectra contain the bands attributable to the characteristic vibrations of the azole ligand coordinated to the silver(I) ion, as well as that due to SbF₆⁻ counter-anion. Thus, the very strong bands at 656, 660 and 655 cm⁻¹ are present in the IR spectra of **1–3**, respectively, being in accordance with no coordination of SbF₆⁻ to the silver(I) ion.²⁹ This is in accordance with the IR spectroscopic data for the previously reported [Ag(1,7-phen)₂]SbF₆ complex (1,7-phen is 1,7-phenanthroline).³⁰ Besides that, the bands at ~3100–3000 cm⁻¹ originate from the C_{aromatic}-H stretching vibrations, while those at ~2900 cm⁻¹ are in accord with the presence of the C_{aliphatic}-H bonds in complexes **1** and **2**.³¹ Moreover, in the IR spectra of all investigated silver(I)-azole complexes, one could observe the bands due to characteristic vibrations of the six- and five-membered aromatic rings ($\nu(\text{C}_{\text{ar}}=\text{C}_{\text{ar}})$ and $\nu(\text{C}=\text{N})$) in the expected region (1618–1406 cm⁻¹).²⁴ As far as complex **2** is concerned, a broad band at 3415 cm⁻¹ in its IR spectra, due to the O–H stretching vibration of voriconazole, is observed.³¹

The ambient temperature UV-vis spectra of silver(I) complexes **1–3** and the corresponding azoles were recorded in DMSO (Fig. S1†). Due to the similarity in the shape of the UV-vis spectra of the silver(I) complex and the respective azole ligand, it can be proposed that the absorbance peaks for the complexes **1–3** at $\lambda_{\text{max}} = 271, 292$ and 260 nm, respectively, originate from the intra-ligand charge transfer transitions.

This is in accordance with the UV-vis spectroscopic features of the previously reported silver(I) complexes with various nitrogen- and sulfur-donor ligands.^{32,33} The absorbance peaks of complexes **1–3** show bathochromic red shifts compared to those of the corresponding azoles ($\lambda_{\text{max}} \sim 255$ nm; see ESI†). The UV-vis spectra were also recorded at 24 and 48 h after dissolution of the complexes **1–3** in DMSO and in DMSO/PBS (PBS is phosphate buffered saline) (Fig. S1 and S2†). No significant changes were seen between the initial UV-vis spectra and those recorded after 48 h (only a slight decrease in the intensity of the absorption maxima of the studied complexes was observed during this period; up to 5% for **1**), being in accordance with the fact that the corresponding azole ligands remains coordinated to the silver(I) ion in solution. Despite this fact, it could be assumed that the silver(I) ion will be released from [Ag(azole)₂]⁺ moiety under the physiological conditions in the presence of proteins and other cellular biomolecules, since the interactions between silver(I) ion and these biomolecules are responsible for its antimicrobial activity.³⁴

The ¹H NMR spectra of silver(I) complexes **1–3** and the respective azoles were recorded in DMSO-*d*₆ (Fig. S3–S5†) and their assignment was performed based on the NMR data reported in the literature for the studied azoles, whose ¹H NMR spectra were recorded in different solvents.^{24,26,35} As can be seen in Fig. S3–S5,† most of the ¹H resonances for the coordinated azoles are downfield shifted concerning those for the uncoordinated ligand. In some cases, the $\Delta(^1\text{H})_{\text{coord}}$ coordination shifts (determined with respect to the azole in DMSO-*d*₆) are not significant, what can be expected for NMR spectroscopic properties of silver(I) complexes in DMSO-*d*₆ solution.^{36,37} In all cases, the largest chemical shift was observed for the proton which is adjacent to the nitrogen binding center, *i.e.* C4H for ecz (+0.18 ppm), C5H for vcz (+0.08 ppm) and C2H for ctz (+0.31 ppm).

The positive ion ESI mass spectra for silver(I) complexes **1–3** (*vide infra*; Fig. S6–S8†) were consistent with the patterns simulated for the corresponding molecular cations, and additionally confirmed the coordination of the corresponding azole to the silver(I) ion in solution.

Computational results

DFT calculations have been carried out to gain a better understanding of the structures of the complexes in DMSO solutions. We have investigated the thermodynamics of possible reactions starting from the X-ray determined structures of the complexes **1–3**. The free energy changes, $\Delta_r G$ (298 K), for the formation of likely coordination structures in solution have been studied (Table 1).^{38,39} $\Delta_r G$ (298 K) was calculated from the difference between the Gibbs free energies of the products and the reactants. A geometry optimization at the ZORA-BP86-D4/TZP-COSMO(DMSO) level of theory was performed. Electronic energies used for the calculation of the Gibbs free energies of studied species were evaluated at two levels of theory – ZORA-MN15/TZ2P-COSMO(DMSO) and ZORA-TPSSH-D4/TZ2P-COSMO(DMSO), and consistent results were obtained



Table 1 Gibbs free energy changes (Δ_rG in kcal mol⁻¹ at $T = 298.15$ K) calculated at ZORA-MN15/TZ2P-COSMO(DMSO)//ZORA-BP86-D4/TZP-COSMO(DMSO) and ZORA-TPSSH-D4/TZ2P-COSMO(DMSO)//ZORA-BP86-D4/TZP-COSMO(DMSO) levels of theory for the formation of different silver(i) complexes

Reaction	Δ_rG (298 K)	
	MN15/ TZ2P	TPSSH-D4/ TZ2P
$[\text{Ag}(\text{ecz})_2]^+ + 2\text{DMSO} \rightleftharpoons [\text{Ag}(\text{DMSO})_2]^+ + 2\text{ecz}$	+9.5	+12.9
$[\text{Ag}(\text{ctz})_2]^+ + 2\text{DMSO} \rightleftharpoons [\text{Ag}(\text{DMSO})_2]^+ + 2\text{ctz}$	+11.2	+14.4
$[\text{Ag}(\text{vcz})_4]^+ \rightleftharpoons [\text{Ag}(\text{vcz})_2]^+ + 2\text{vcz}$	-2.3	-2.6
$[\text{Ag}(\text{vcz})_2]^+ + 2\text{DMSO} \rightleftharpoons [\text{Ag}(\text{DMSO})_2]^+ + 2\text{vcz}$	+3.1	+7.0

(Table 1). Complexes **1** and **3** are stable in DMSO solution, maintaining their linear coordination with twoazole ligands coordinated in a monodentate fashion (Fig. 3). In the case of the polymeric structure **2**, the tetracoordinated complex $[\text{Ag}(\text{vcz})_4]^+$ was the starting point for the computational analysis. It was found that the dissociation of two vcz ligands is thermodynamically favored, leading to the linear $[\text{Ag}(\text{vcz})_2]^+$ (Fig. 3 and Table 1). The $[\text{Ag}(\text{vcz})_2]^+$ species is stable in DMSO solution, similar to complexes **1** and **3** (Table 1). Thus, based on our calculations, all three complexes are ascertained as $[\text{Ag}(\text{azole})_2]^+$ in DMSO solution (Fig. 3), with twoazole ligands linearly coordinated to the silver(i) center, corroborating spectroscopic results.

Electrochemical behavior

To better understand the stability and biological activity of a redox active compound both *in vitro* and *in vivo*, it is very important to investigate its redox properties. Cyclic voltammetry determines the potential at which the compound can be reduced and/or oxidized.⁴⁰ Thus, the cyclic voltammograms of the presently synthesized complexes were recorded at the glassy carbon (GC) electrode in DMSO and 0.1 M tetrabutylammonium hexafluorophosphate (TBAHP) as a supporting electrolyte under the following conditions, $E_{\text{begin}} = -2.0$ V, $E_{\text{end}} = 2.0$ V, scan rate = 50 mV s⁻¹ (Fig. S9†). In the voltammograms of the complexes **1–3**, one oxidation peak I_a at ~1.27, 1.48 and 1.47 V, respectively, was observed, which was attributed to the

oxidation of silver(i) to silver(ii) in accordance with the previous reports for the redox active silver(i) complexes.^{41–43} In cathodic direction, two reduction peaks $I_{c,1}$ and $I_{c,2}$ (at ~-0.28 and -0.92 V for **1**; at ~-0.40 and -1.04 V for **2** and **3**; Fig. S9†) are visible in the cyclic voltammograms of the complexes and are due to the reduction processes silver(ii) → silver(i) and silver(i) → silver(0), respectively.^{41–43} It is important to note that silver can exert biological activity in all these oxidation states.^{44–46}

Evaluation of biological activity of silver(i) complexes 1–3

Antimicrobial and antiproliferative activities. The antimicrobial potential of silver(i) complexes is well known, and recent studies have also demonstrated their cytotoxic and genotoxic potential toward normal and cancer cells.^{47,48} In comparison to simple silver(i) salt, it was found that silver(i) complexes with organic-based ligands exhibit more varied chemical properties.⁴⁷ Moreover, the use of simple silver(i) salts has been limited since they undergo fast dissociation, leading to the precipitation of AgCl under physiological conditions, a process that prevents the antimicrobial action of silver(i) ion in accordance with the pathways previously described.³⁴

To determine the influence of the coordinated silver(i) ion on the antimicrobial activity of complexes **1–3**, the biological properties of these complexes were compared with those of the corresponding antifungal azoles (Table 2). The investigated silver(i)-azole complexes **1–3** have shown excellent antifungal and good to moderate antibacterial activities. In comparison to the uncoordinated vcz and ctz azoles, complexes **2** and **3**, respectively, exhibited significantly better antifungal activity, whereby **2** showed increased activity of 30-fold (*C. parapsilosis*), 75-fold (*C. albicans*), 140-fold (*C. krusei*) and 9533-fold (*C. glabrata*) in comparison to vcz, while **3** showed increased activity of 9-fold (*C. glabrata*), 22-fold (*C. albicans*), 47-fold (*C. krusei*) and 1020-fold (*C. parapsilosis*) in comparison to ctz. An improved antifungal activity was also observed for complex **1** in comparison to ecz against all tested strains except *C. krusei*, but this effect was less significant (1.7- to 5.0-fold).

The obtained results are in line with those previously achieved by complexation of icz with silver(i) ion, whereby $[\text{Ag}(\text{icz})_2]\text{NO}_3 \cdot \text{H}_2\text{O}$ complex is 2.3- and 4.5-fold more active than

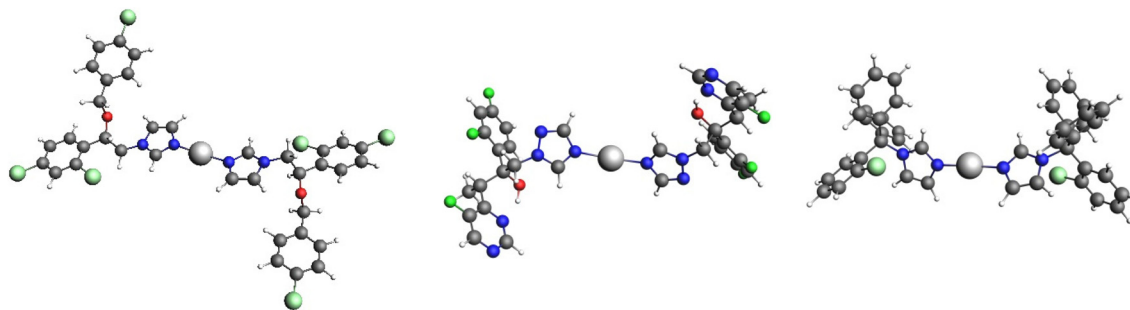


Fig. 3 The structures of $[\text{Ag}(\text{ecz})_2]^+$ (left), $[\text{Ag}(\text{vcz})_2]^+$ (middle) and $[\text{Ag}(\text{ctz})_2]^+$ (right) optimized at the ZORA-BP86-D4/TZP-COSMO(DMSO) level of theory.



Table 2 Antimicrobial activity (MIC, μM) of silver(i) complexes 1–3, the corresponding azoles and AgSbF_6 against *Candida* and bacterial strains in comparison to their antiproliferative activity (IC_{50} , μM)^a

	1	2	3	ecz	vcz	ctz	AgSbF_6
<i>C. albicans</i> ATCC 10231	2.25 \pm 0.10	0.48 \pm 0.02	0.12 \pm 0.03	7.00 \pm 0.14	35.80 \pm 0.29	2.60 \pm 0.15	3.64 \pm 0.20
<i>C. parapsilosis</i> ATCC 22019	2.25 \pm 0.11	0.01 \pm 0.001	0.01 \pm 0.001	3.90 \pm 0.19	0.30 \pm 0.09	10.20 \pm 0.28	0.09 \pm 0.01
<i>C. krusei</i> ATCC 6258	27.10 \pm 0.15	0.01 \pm 0.001	0.03 \pm 0.01	14.10 \pm 0.23	1.40 \pm 0.08	1.40 \pm 0.09	4.66 \pm 0.19
<i>C. glabrata</i> ATCC 2001	11.29 \pm 0.25	0.06 \pm 0.01	0.97 \pm 0.06	56.20 \pm 0.13	572.00 \pm 0.01	9.10 \pm 0.19	2.33 \pm 0.07
<i>P. aeruginosa</i> NCTC 10332	22.6 \pm 0.22	11.9 \pm 0.21	12.1 \pm 0.22	>500	>500	>500	36.38 \pm 0.11
<i>E. coli</i> NCTC 2001	11.3 \pm 0.15	23.9 \pm 0.25	12.1 \pm 0.17	>500	>500	>500	18.19 \pm 0.15
<i>S. aureus</i> ATCC 25923	2.71 \pm 0.14	47.9 \pm 0.25	2.61 \pm 0.20	225.00 \pm 0.01	>500	290.00 \pm 0.02	36.38 \pm 0.07
<i>L. monocytogenes</i> NCTC 11994	22.6 \pm 0.15	47.9 \pm 0.16	12.1 \pm 0.27	>500	>500	>500	36.38 \pm 0.22
MRC-5 cells	10.0 \pm 1.0	36.1 \pm 1.5	16.0 \pm 0.9	10.3 \pm 1.0	859.0 \pm 5.0	8.7 \pm 0.4	18.3 \pm 0.3

^a IC_{50} is the concentration of a compound, which inhibits 50% of cell growth after treatment of 48 h.

icz against *C. albicans* and *C. glabrata*.²³ Moreover, the previously reported silver(i) complexes with vcz, $[\text{Ag}(\text{vcz})_2]_n(\text{ClO}_4)_n$ and $[\text{Ag}_2(\text{vcz})_4]_n(\text{NO}_3)_{2n}$,²⁷ have shown an improvement in the activity against the panel of *Candida* spp., including vcz resistant isolates. The MIC values (μM) for the corresponding salt used for their synthesis, AgSbF_6 , are also given in Table 2 and although these values are comparable to the effect of the analyzed antifungal drugs, as well as the corresponding silver(i) complexes, its potential application is limited because this salt undergoes fast dissociation leading to the formation of AgCl precipitate under physiological conditions, as was mentioned above.³⁴

The complexation of different organic ligands with silver(i) ion led to the formation of complexes, which also possess significant antibacterial activity.^{34,49,50} In comparison to the uncoordinated azoles, silver(i)-azoles complexes 1–3 exhibited significantly better antibacterial activity against all tested strains, ranging from 2.61–47.9 μM (Table 2). All investigated silver(i)-azole complexes had antibacterial activity, with the best activity observed for 1 and 3 against Gram-positive *S. aureus*, at 2.71 and 2.61 μM , respectively. Interestingly, when tested alone, two of the azole ligands which are in use for antifungal treatment in clinical practice (ecz and ctz), also had an effect against the same bacterial strain, while vcz was inactive against *S. aureus* at tested concentrations (among the complexes, 2 exhibited the lowest antibacterial activity). None of the uncoordinated azoles has shown antibacterial activity against other tested bacterial strains.

When cytotoxicity of the novel silver(i)-azole complexes against healthy human fibroblasts (MRC-5) was analyzed, it was observed that complex 1 exhibited a comparable effect to ecz, 2 was 24-fold more cytotoxic compared to vcz, while only 3 had a more favorable toxicity profile compared to ctz (1.8-fold lower) (Table 2). The selectivity index (SI) was determined for silver(i) complexes 1–3 and the corresponding azoles by dividing the obtained IC_{50} with MIC value (Table S1†). The SI values for the complexes on the tested *Candida* strains are in the range from exceptionally high at 3610 (2 for *C. parapsilosis* and *C. krusei*) to 0.4 (1 for *C. krusei*). For instance, clinically used silver(i) sulfadiazine, AgSD , has the highest SI of 4 against *C. parapsilosis* and *C. krusei*.⁵¹

Considering that clinical azoles are known to interfere with ergosterol biosynthesis by inhibiting the cytochrome P450,⁵² we have investigated the effect of complexes 2 and 3, the corresponding azoles vcz and ctz, and AgSbF_6 on this process (Fig. S10†). In accordance with this, the ergosterol levels in *C. albicans* ATCC 10231 treated with these compounds were assessed. As can be seen from Fig. S10,† complexes 2 and 3 significantly reduced the ergosterol levels at $0.5 \times \text{MIC}$, while vcz and ctz, as well as AgSbF_6 , did not reduce or slightly reduced the ergosterol levels at the same concentration, compared to the untreated control (*C. albicans* ATCC 10231). These results reveal that the inhibition of ergosterol biosynthesis in the presence of complexes 2 and 3 is in correlation with the results of their antimicrobial activity.

Filamentation test on *C. albicans* ATCC 10231. The morphological transformation from yeast to hyphae form of *C. albicans* is one of the important aspects of its pathogenesis.⁵³ Recently, we have revealed that the presence of different silver(i) complexes can inhibit the cellular differentiation of *Candida*.^{30,54} Therefore, the effects of $0.5 \times \text{MIC}$ concentrations of novel silver(i)-azole complexes 2 and 3, which showed excellent MIC values against *C. albicans* ATCC 10231 (Table 2), together with corresponding azoles vcz and ctz, respectively, on *C. albicans* hyphae formation was studied. All tested compounds were able to completely prevent hyphae formation on the solid medium, even during prolonged exposure up to 72 h (Fig. 4).

Antibiofilm activity assessment on *C. albicans* ATCC 10231. Yeast to hyphae transition is an important process during the infection process, and it is also the early step in *Candida* biofilm formation.⁵⁵ Therefore, it is of great importance to evaluate the antibiofilm activity of novel silver(i)-azole complexes with respect to the high level of resistance of biofilms to conventional drugs. Complexes 2 and 3 inhibited the formation of *Candida* biofilms at $0.5 \times \text{MIC}$ value in high percentages of 87 and 86%, respectively (Table S2†). In comparison to the corresponding azoles, vcz and ctz (62 and 79%, respectively), biofilm formation inhibition was elevated for the corresponding complexes 2 and 3, respectively, suggesting the beneficial effect of the presence of the silver(i) ion. The AgSbF_6 used for the synthesis of the complexes has induced a similar



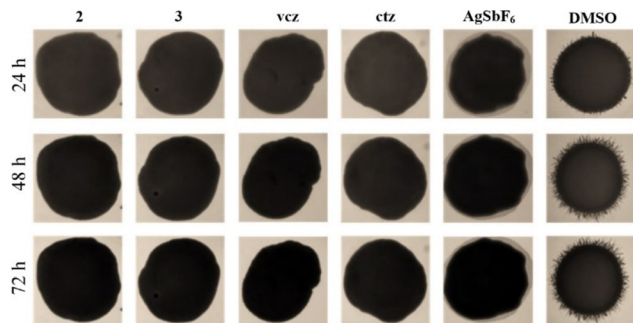


Fig. 4 Yeast to hyphae transition of *C. albicans* ATCC 10231 strain treated with 0.5 \times MIC of the tested compounds after 24, 48 and 72 h compared to the DMSO control.

biofilm formation inhibition. On the other hand, none of the tested compounds has destroyed the already formed *C. albicans* biofilms (data not shown).

Adherence assay. To study the effects on *Candida* pathogenesis more thoroughly, the effect on *C. albicans* adherence to A549 cells was analyzed (Fig. 5). These cells were shown to be susceptible and permissive for infection, since they exhibit mucin overexpression and were used as promising models for studying *in vitro* infections using both bacteria and fungi.^{56–58} The adherence of pathogenic fungi to human cells is considered as the initial step in the invasion of host cells. First, it was shown that the lowest MIC against fluorescently labelled *C. albicans* SC5314-RFP, used in the adherence assay, was determined for **3** (0.31 μ M, data not shown), so this complex and the corresponding ctz ligand were selected for further analysis. In DMSO control, *C. albicans* cells in the filamentous form, attached to A549 monolayer are clearly visible (Fig. 5a). Comparable, but slightly less filamentous SC5314-RFP adherence compared to the DMSO control was observed for complex **3** (Fig. 5b), while the most pronounced reduction in the adhesion of SC5314-RFP cells was observed for ctz (Fig. 5c). Notably smaller and more brightly stained nuclei were observed for A549 monolayer treated with complex **3**, after staining with DAPI (2-(4-aminophenyl)-6-indolecarbamidine dihydrochloride). This is an indication that A549 cells were dead before fixation, since DAPI is commonly used to analyze

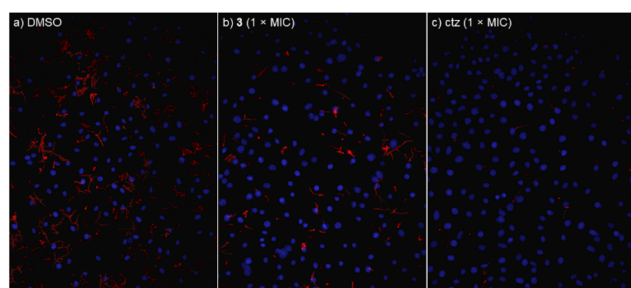


Fig. 5 Infection of A549 cells (blue stained nuclei) with *C. albicans* SC5314-RFP (red) in the presence of (a) DMSO, (b) complex **3** at 1 \times MIC, (c) ctz at 1 \times MIC value concentrations at 20 \times magnification.

nuclear morphologic changes such as chromosome condensation in apoptotic cells. The concentration of complex **3** employed in the adherence assay was over 100 times lower than the IC₅₀ value determined in the antiproliferative assay with MRC-5 cells (SI 133.3; Table S1†). This indicates a higher sensitivity of A549 cancer cells to complex **3** compared to normal fibroblasts and points out that this complex could be further tested in cytotoxicity assays against various cancer cell lines. Compounds that simultaneously exert different types of biological activities (*e.g.*, anticancer, antifungal, antibacterial) are especially interesting since anticancer chemotherapy commonly weakens the immune system and protection against infections is welcome.^{59,60}

Experimental

Materials and measurements

Silver(i) hexafluoroantimonate(v) (AgSbF₆), econazole (ecz), voriconazole (vcz), clotrimazole (ctz), ethanol, acetonitrile, dimethyl sulfoxide (DMSO) and deuterated dimethyl sulfoxide (DMSO-*d*₆) were obtained from the commercial suppliers (Sigma-Aldrich and Acros Organics). All chemicals were of analytical grade and used without further purification. Solvents were used as received.

Elemental analyses of the synthesized silver(i)-azole complexes **1–3** for carbon, hydrogen and nitrogen were performed using a PerkinElmer 2400 Series II instrument (CHN). The ESI-HRMS spectra in the positive mode were recorded after dissolving the corresponding compound in CH₃CN with an Agilent 62224 accurate mass spectrometer, using time of flight liquid chromatography/mass spectrometry. The IR spectra were recorded on a PerkinElmer Spectrum 2 spectrometer by KBr pellet technique over the wavenumber range of 4000–450 cm⁻¹ (abbreviations used: br for broad, vs for very strong, s for strong, m for medium, w for weak). The UV-vis spectra were recorded over the wavelength range of 1100–200 nm on a Shimadzu UV-1800 spectrophotometer at ambient temperature. The concentration of DMSO solutions for UV-vis measurements was 6.4 \times 10⁻⁴ M (**1**), 7.4 \times 10⁻⁴ M (**2**) and 4.8 \times 10⁻⁴ M (**3**). Additionally, the measurement of the UV-vis spectra for **1–3** was repeated after 24 and 48 h standing in the dark at ambient temperature. Moreover, the solution behavior of complexes **1–3** was studied by UV-vis measurements in DMSO/PBS (*v/v* is 7 : 3) during 48 h at ambient temperature. The ¹H NMR spectra of silver(i) complexes **1–3** and the corresponding azoles were recorded on a Varian Gemini 2000 spectrometer at 200 MHz at ambient temperature. 5.0 mg of each compound was dissolved in 0.6 mL of DMSO-*d*₆ and transferred into a 5 mm NMR tube. Chemical shifts, σ , are reported in ppm (parts per million) and scalar couplings, *J*, are given in Hz (Hertz). The splitting of protons is designated as: s, singlet; d, doublet; dd, doublet of doublets; dt, doublet of triplets; t, triplet; td, triplet of doublets; q, quartet and m, multiplet. The cyclic voltammetry (CV) measurements were performed using a potentiostat/galvanostat AutoLab



PGSTAT204 (Utrecht, Netherlands). The three-electrode system consisted of a glassy carbon (GC) electrode as a working electrode, Ag/AgCl (saturated KCl) as a reference electrode and a platinum wire as a counter electrode. The electrode surface was renewed before each measurement by polishing with Al₂O₃ micro-powder and with a piece of cotton due to the strong adsorption of the complex. The concentration of the solution of the complexes in DMSO used for these measurements was 1.0×10^{-3} M.

Data from single crystals of 1–3 (Fig. S11 and S12[†]) were collected at 150 K on a SuperNova diffractometer with Atlas detector using CrysAlis software with monochromated Mo K α (0.71073 Å).⁶¹ The initial structural models were solved with direct methods implemented in SHELXT using the Olex2 graphical user interface.⁶² A full-matrix least-squares refinement on F^2 magnitudes with anisotropic displacement parameters for all non-hydrogen atoms using Olex2 or SHELXL-2018/3 was performed.^{62,63} All non-hydrogen atoms were refined anisotropically, while hydrogen atoms were placed at calculated positions and treated as riding on their parent atoms. Further details on the crystal data, data acquisition and refinement are given in Table S3.[†] Figures were prepared with Mercury.⁶⁴

Synthesis of silver(I) complexes 1–3

Silver(I) complexes 1–3 were synthesized by modification of the previously reported procedure for the synthesis of silver(I) complex with itraconazole.²³ The solution of 0.5 mmol of the corresponding azole (190.8 mg of ecz for 1, 174.6 mg of vcz for 2 and 172.4 mg of ctz for 3) in 10.0 mL of ethanol was added slowly under stirring to the solution containing an equimolar amount of AgSbF₆ (171.8 mg) dissolved in 5.0 mL of ethanol. The obtained solutions were mixed at ambient temperature for 3 h in the absence of light. The crystals of complex 1 were obtained after the white precipitate from the reaction was recrystallized in acetonitrile, while the crystals of 2 and 3 were formed by recrystallization of the resulting white precipitates in acetonitrile/ethanol (v/v 1:1) and after evaporation at ambient temperature for 3–5 days. The obtained crystals were filtered off and dried in the dark at room temperature. Yield: 210.3 mg (76%) for 1, 185.0 mg (71%) for 2 and 188.6 mg (73%) for 3.

Anal. calcd for 1 (C₃₆H₃₀AgCl₆F₆N₄O₂Sb; M_w = 1106.96 g mol⁻¹): C, 39.06; H, 2.73; N, 5.06. Found: C, 39.35; H, 2.79; N, 5.43%. HRMS-ESI (CH₃CN): m/z calcd for [Ag(ecz)₂]⁺ [C₃₆H₃₀AgCl₆N₄O₂]⁺: 866.9545; found 866.9583. IR (KBr, ν , cm⁻¹): 3146m, 3101w, 3090w, 3072w, 3051m (ν (C_{diazole}-H) and ν (C_{ar}-H)), 2939w, 2899w, 2871w, 2861w (ν (C-H)), 1599m, 1589m, 1561m, 1524s, 1492s, 1470s, 1439m, 1407m (ν (C_{ar}=C_{ar}) and ν (C=N)), 1246m, 1225m (β (C_{ar}-H) and β (C_{diazole}-H)), 1109s (ν (C-O)), 1094vs (ν (C_{ar}-Cl)), 838m, 830m, 819m, 810m, 788m, 761m, 720w, 696w (γ (C_{ar}-H)) and (γ (C_{diazole}-H)), 656vs (ν (SbF₆)). ¹H NMR (200 MHz, DMSO-*d*₆): δ 7.80 (s, 1H, C2H), 7.68 (*d*, J = 2.0 Hz, 1H, C4H), 7.48 (*dd*, J = 8.4, 2.0 Hz, 1H, C10H), 7.37 (*dd*, J = 7.3, 5.2 Hz, 2H, C5H, C13H), 7.33 (s, 1H, C12H), 7.22 (s, 1H, C17H), 7.20 (s, 1H,

C19H), 7.16 (s, 1H, C16H), 7.01 (s, 1H, C20H), 5.01 (*t*, J = 5.3 Hz, 1H, C7H), 4.40 (*m*, 2H, C6H), 4.29 ppm (*d*, J = 12.4 Hz, 2H, C14H). UV-vis (DMSO, λ_{\max} , nm): 271 (ϵ = 1.2×10^3 M⁻¹ cm⁻¹).

Anal. calcd for 2 (C₃₂H₂₈AgF₁₂N₁₀O₂Sb; M_w = 1042.26 g mol⁻¹): C, 36.88; H, 2.71; N, 13.44. Found: C, 36.79; H, 2.68; N, 13.38%. HRMS-ESI (CH₃CN): m/z calcd for [Ag(vcz)(MeCN)]⁺ [C₁₈H₁₇AgF₃N₆O]⁺: 497.0467; found 497.0447. IR (KBr, ν , cm⁻¹): 3415br (ν (O-H)), 3192w (ν (C_{ar}-H)), 2992w, 2943w, 2976w (ν (C-H)), 1618s, 1596s, 1524m, 1499s, 1457m, 1423m, 1406vs (ν (C_{ar}=C_{ar}) and ν (C=N)), 1291m (δ (O-H)), 1242w, 1218w (β (C_{ar}-H) and β (C_{triazole}-H)), 1132m (ν (C-F)), 966m (ν (C-O)), 852m, 827w, 804w, 781w, 756w, 737w (γ (C_{ar}-H)) and (γ (C_{triazole}-H)), 660vs (ν (SbF₆)), 622m (β (C_{ar}-F)). ¹H NMR (200 MHz, DMSO-*d*₆): δ = 9.06 (*d*, J = 2.9 Hz, 1H, C18H), 8.87 (*d*, J = 2.1 Hz, 1H, C20H), 8.32 (s, 1H, C5H), 7.68 (s, 1H, C3H), 7.27 (*m*, 1H, C9H), 7.18 (*m*, 1H, C12H), 6.93 (*td*, J = 8.5, 2.5 Hz, 1H, C10H), 6.01 (s, 1H, OH), 4.83 (*d*, J = 14.3 Hz, 1H, C6H), 4.36 (*d*, J = 14.2 Hz, 1H, C6H), 3.94 (*q*, J = 7.0 Hz, 1H, C14H), 1.12 ppm (*d*, J = 7.0 Hz, 3H, C15H). UV-vis (DMSO, λ_{\max} , nm): 292 (ϵ = 1.1×10^3 M⁻¹ cm⁻¹).

Anal. calcd for 3 (C₄₄H₃₄AgCl₂F₆N₄Sb; M_w = 1033.27 g mol⁻¹): C, 51.14; H, 3.32; N, 5.42. Found: C, 51.07; H, 3.35; N, 5.35%. HRMS-ESI (CH₃CN): m/z calcd for [Ag(ctz)₂]⁺ [C₄₄H₃₄AgCl₂N₄]⁺: 795.1206; found 795.1209. IR (KBr, ν , cm⁻¹): 3177w, 3162w, 3140w, 3108w, 3089w, 3037w (ν (C_{triazole}-H) and ν (C_{ar}-H)), 2927w (ν (C-H)), 1603w, 1568w, 1530w, 1505m, 1495 m, 1465w, 1447m, 1433m (ν (C_{ar}=C_{ar}) and ν (C_{ar}=N)), 1276m, 1225m (β (C_{ar}-H)) and β (C_{diazole}-H)), 1130m (ν (C-O)), 1093s (ν (C_{ar}-Cl)), 765s, 753s, 748s (γ (C_{ar}-H)), 655vs (ν (SbF₆)), 633m (γ (C_{ar}-H)). ¹H NMR (200 MHz, DMSO-*d*₆): δ = 7.83 (s, 1H, C2H), 7.57 (*dd*, J = 7.7, 2.0 Hz, 1H, C8H), 7.51 (*d*, J = 1.7 Hz, 1H, C10H), 7.46 (*m*, 2H, C14H, C15H), 7.42 (*m*, 5H, C9H, C16H, C20H, C21H, C22H), 7.15 (*m*, 1H, C13H), 7.09 (*m*, 3H, C17H, C19H, C23H), 7.06 (*d*, J = 1.7 Hz, 2H, C4H, C5H), 6.94 ppm (*dd*, J = 7.7, 1.5 Hz, 1H, C11H). UV-vis (DMSO, λ_{\max} , nm): 260 (ϵ = 1.7×10^3 M⁻¹ cm⁻¹).

For comparative purposes, the corresponding azoles were characterized by ¹H NMR, IR and UV-vis spectroscopy and these data are given in ESI.[†]

Computational details

All DFT calculations were done with the ADF⁶⁵ engine in the Amsterdam Modeling Suite (version 2023.104).⁶⁶ The scalar-relativistic Zeroth Order Regular Approximation (ZORA) was used to account for relativistic effects.^{67–69} The COSMO solvation model,^{70,71} as implemented in ADF,⁷² with DMSO as solvent was used in all calculations. Geometry optimizations were performed with the BP86 exchange–correlation functional,^{73–75} with Grimme's fourth generation dispersion energy corrections,⁷⁶ *i.e.*, BP86-D4. The all-electron triple-zeta Slater-type orbitals plus one polarization function (TZP) basis set was used for all atoms. The harmonic frequencies were calculated at the same level of theory. Vibrational analysis with low vibrational frequency free rotor interpolation corrections, as proposed by Li/Head-Gordon⁷⁷ and Grimme⁷⁸ has been used to evaluate internal energies and entropic effects to the



Gibbs free energy at 298 K (frequency cut-off 100 cm^{-1}). Correction due to the standard state conversion (1 atm. to 1 mol dm^{-3} solution standard state) is applied ($1.89\text{ kcal mol}^{-1}$ to the free energies at 298 K). For DMSO, the free energy correction due to the conversion to the solvent standard state is made ($3.46\text{ kcal mol}^{-1}$, at 298.15 K). Electronic energies used to calculate the Gibbs free energy were evaluated with MN15⁷⁹ and TPSSH-D4^{76,80,81} meta-hybrid functionals at ZORA-BP86-D4/TZP-COSMO(DMSO) geometries. The all-electron triple-zeta Slater-type orbitals with two polarization functions (TZ2P) basis set were used for all atoms to calculate electronic energies. The LibXC library⁸² was used for all calculations employing MN15 functional.

Antimicrobial activity

Minimum inhibitory concentration (MIC) values of the complexes 1–3, AgSbF₆, and the corresponding azoles were determined according to the standard broth microdilution assays, recommended by the National Committee for Clinical Laboratory Standards (M07-A8) for bacteria and Standards of the European Committee on Antimicrobial Susceptibility Testing (v 7.3.1: Method for the determination of broth dilution minimum inhibitory concentrations of antifungal agents for yeasts) for *Candida* spp.⁸³ The tested compounds were dissolved in DMSO at a concentration of 50 mg mL^{-1} . The highest concentration used for antifungal testing was 250 mg mL^{-1} , and for antibacterial testing was 200 mg mL^{-1} . The tested microorganisms included four fungal *Candida* strains obtained from the American Type Culture Collection (ATCC): *C. albicans* ATCC 10231, *C. parapsilosis* ATCC 22019, *C. krusei* ATCC 6258 and *C. glabrata* ATCC 2001, and four bacterial strains: *Pseudomonas aeruginosa* PAO1 NCTC 10332, *Escherichia coli* NCTC 2001, *Staphylococcus aureus* ATCC 25923 and *Listeria monocytogenes* NCTC 11994. The inoculums were 1×10^5 colony forming units (cfu) mL^{-1} for *Candida* species and 5×10^5 cfu mL^{-1} for bacteria. The MIC value was recorded as the lowest concentration that inhibited the growth after 24 h at 37 °C, using a plate reader (Epoch Microplate Spectrophotometer, BioTek Instruments, Inc., USA).

Cell viability and proliferation assay

Antiproliferative activity was measured using the standard colorimetric MTT assay.⁸⁴ Briefly, cells were plated in a 96-well flat-bottomed microtiter plate at a concentration of 1×10^4 cells per well, grown in a humidified atmosphere of 95% air with 5% CO₂ at 37 °C and maintained as monolayer cultures in RPMI 1640 medium supplemented with 10% fetal bovine serum (FBS), 100 U mL^{-1} penicillin and 100 $\mu\text{g mL}^{-1}$ streptomycin. Serial dilutions of each tested compound were added to the cells, starting with 50 μM as the maximum concentration. In the case of vcz, the maximum tested concentration was 1000 μM . The treatment lasted for 48 h. The MTT assay was performed two times in four replicates and the results were presented as a percentage of the DMSO-treated control that was arbitrarily set to 100%. The extent of MTT reduction was measured spectrophotometrically at 540 nm using a plate

reader (Epoch Microplate Spectrophotometer, BioTek Instruments, Inc., USA). Cytotoxicity was expressed as the concentration of compound inhibiting the cell growth by 50% (IC₅₀) in comparison with the negative control (DMSO-treated cells).

Ergosterol analysis

Ergosterol levels were measured in untreated cultures of *C. albicans* ATCC 10231 and cultures treated with $0.5 \times \text{MIC}$ of AgSbF₆, azoles vcz and ctz, and complexes 2 and 3 after 18 h incubation at 37 °C on the rotary shaker (180 rpm) following the procedure.⁸⁵ Ultrospec 3300pro 573 (Amersham Biosciences, Amersham, UK), spectrophotometer was used for following the ergosterol levels (concentrations) by scanning absorbance between 240 and 300 nm.

Filamentation test on *C. albicans* ATCC 10231

The effect of the tested compounds on *C. albicans* ATCC 10231 hyphae formation was assessed using solid composition.⁸⁶ Briefly, 1 mL of *C. albicans* cells from an overnight culture grown in Sabouraud dextrose broth medium at 37 °C were centrifuged for 10 min at 16.873 rcf, and the pellet was washed several times with sterile PBS (phosphate-buffered saline; Sigma Aldrich, Munich, Germany). The pellet was resuspended in 200 μL PBS, and 2 μL of the cell suspension was poured over the solid composition with or without the tested compounds and incubated at 37 °C for 72 h. Morphological changes of *C. albicans* ATCC 10231 in the presence of subinhibitory concentration ($0.5 \times \text{MIC}$) of compounds or without them were analyzed using bright field microscopy (SMZ143-N2GG, Motic, Germany). *C. albicans* ATCC 10231 treated with DMSO was used as a control.

Anti-biofilm activity assessment on *C. albicans* ATCC 10231

The effect of the tested compounds on biofilm formation and disruption of preformed biofilms was determined on the *C. albicans* ATCC 10231 strain. Antibiofilm assays were conducted using previously reported methodologies.^{41,87} Briefly, the assays were carried out in 96-well round-bottom polystyrene microtiter plates. Cells were harvested from overnight grown cultures, washed twice with sterile PBS, and resuspended in RPMI 1640 medium (Sigma Aldrich, Munich, Germany) containing 2% glucose (w/v) at a concentration of 1×10^5 cfu mL^{-1} . *C. albicans* suspension was incubated with $0.5 \times \text{MIC}$ in 200 μL final volume per well for 48 h at 37 °C to allow biofilm formation. Biofilm growth was analyzed by crystal violet (CV) staining of adherent cells and the absorbance at 590 nm was read by a plate reader (Epoch Microplate Spectrophotometer, BioTek Instruments, Inc., USA). In the biofilm disruption assay, preformed biofilms (24 h at 37 °C) were incubated for 24 h with decreasing concentrations of the compound. Biofilm growth was quantified by CV staining of adherent cells and estimated as absorbance at 530 nm on an Epoch Microplate Spectrophotometer, BioTek Instruments, Inc.



Adherence assay

The ability of red fluorescence protein (RFP)-labeled *C. albicans* SC5314 cells to infect human adenocarcinoma alveolar basal epithelial cells A549 (obtained from ATCC) was tested in an adherence assay, as described previously.^{88,89} A549 cells were grown on 22 mm glass coverslips in RPMI 1640 medium for two days. Overnight culture of *C. albicans* SC5314-RFP grown in Sabouraud dextrose broth medium at 37 °C was centrifuged for 10 min at 16.873 rcf. The pellet was washed several times with sterile PBS, 50 µL was inoculated into 5 mL RPMI 1640 medium without FBS or any antibiotic and grown at 37 °C to $A_{530} = 0.2$ ($A_{530} = 0.3$ corresponds to $1.0\text{--}2.5 \times 10^6$ cells per mL). A549 monolayers on glass coverslips were inoculated with $\sim 1 \times 10^6$ *C. albicans* cells in the log growth phase (without centrifugation) and co-incubated with the selected compounds added at concentrations of $0.5 \times \text{MIC}$ and $1 \times \text{MIC}$ for 1.5 h in RPMI 1640 without FBS at 37 °C and 5% CO₂. After co-incubation, non-adherent cells were removed by extensively rinsing three times with PBS and samples fixed with 4% *p*-formaldehyde. Next, A549 cells were stained with $1 \mu\text{g mL}^{-1}$ of 2-(4-amidinophenyl)-6-indolecarbamidine dihydrochloride (DAPI, Sigma Aldrich, Munich, Germany) for 10 min in the dark. Both A549 and *C. albicans* SC5314-RFP cells were visualized using a fluorescence microscope (Olympus BX51, Applied Imaging Corp., San Jose, USA) at $20\times$ magnification.

Statistical analysis

The results are presented as mean \pm standard deviation (SD). Statistical analysis was done by comparing means using *t*-test (Two-Sample Assuming Equal Variances) and one-way ANalysis of VAriance (ANOVA, Single Factor), with Fisher's Least Significant Difference (LSD) *post-hoc* test. The level of statistical significance is expressed as a *p*-value (probability value), and $p \leq 0.05$ was considered statistically significant. Statistical analysis tests were performed in Microsoft Excel Spreadsheet Software by Data Analysis Tools add-in.

Conclusions

The investigation of the reactions of silver(I) salt, AgSbF₆, with econazole (ecz), voriconazole (vcz) and clotrimazole (ctz) has shown that silver(I) ion has good coordinating abilities for these clinically used antifungal azoles. The geometry of the silver(I)-azole complexes in the solid state depends on the structural features of the coordinating azole. Thus, the coordination of silver(I) ion with ecz and ctz, both containing imidazole ring, leads to the formation of mononuclear complexes of linear geometry, [Ag(ecz)₂]SbF₆ (1) and [Ag(ctz)₂]SbF₆ (3), respectively. However, the reaction of silver(I) ion with vcz, containing a triazole ring, results in formation of polymeric {[Ag(vcz)₂]SbF₆}_{*n*} complex (2), in which silver(I) ions are coordinated by four nitrogen atoms and adopt a distorted tetrahedral geometry. Nevertheless, in the case of the latter complex, the formation of [Ag(vcz)₂]⁺ species is favored in solu-

tion. The most important finding from the *in vitro* antimicrobial activity and toxicity evaluation is the fact that the synthesized complexes 1–3 have shown an improved anti-*Candida* activity and therapeutic profile in comparison to the corresponding clinically used antifungal azoles (with an increase of activity by up to five orders of magnitude). Moreover, the coordination of silver(I) ion to the azoles has endowed them also with antibacterial activity. Furthermore, the silver(I)-azole complexes have significantly contributed to the inhibition of the formation of *C. albicans* hyphae and biofilms at their subinhibitory concentration, which is a highly desirable property for a new antimicrobial agent. Taken all these facts together, it can be concluded that compounds obtained from the complexation reaction of the metal ion with antifungal azoles deserve further consideration as potential new antifungal agents with favorable pharmacological properties, being more effective and safer than the clinically used antifungal azoles in the treatment of lethal *Candida* infections.

Author contributions

Conceptualization, M. S., J. N. R., I. T., M. I. Dj. and B. Đ. G.; methodology, M. S., J. K. and S. V.; software, J. K. and M. Z.; validation, J. N. R., I. T., M. I. Dj. and B. Đ. G.; investigation, M. S., J. K., N. Lj. S., M. Z., J. L., S. S. B. and S. V.; resources, J. N. R., M. Z., I. T., M. I. Dj. and B. Đ. G.; writing – original draft preparation, J. K., N. Lj. S., M. Z., J. L., S. S. B. and S. V.; writing – review and editing, J. N. R., I. T., M. I. Dj. and B. Đ. G.; visualization, M. S., J. K., N. Lj. S., M. Z., J. L. and S. S. B.; supervision, I. T., M. I. Dj. and B. Đ. G. All authors read and approved the final manuscript.

Conflicts of interest

The authors declare no conflicts of interest.

Acknowledgements

This research has been financially supported by the Ministry of Science, Technological Development and Innovation of the Republic of Serbia (Agreements No. 451–03–47/2023–01/200026, 451-03-47/2023-01/200042 and 451-03-47/2023-01/200122) and by the Centre for Research Infrastructure at the University of Ljubljana, Faculty of Chemistry and Chemical Technology, which is part of the Network of Research and Infrastructural Centres UL (MRIC UL) financially supported by the Slovenian Research Agency (grant P1-0175 and Infrastructure programme No. IO-0022). The EN → FIST Centre of Excellence, Trg OF 13, SI-1000 Ljubljana, Slovenia, is acknowledged for the use of the SuperNova diffractometer. We thank Marta Počkaj for advice on modelling and refining the disordered atoms in crystal structures. This research has also received funding from the Serbian Academy of Sciences and Arts under project No. F128. N. Lj. S. is gratefully acknowl-



edged to the Ministry of Education, Science and Sport of the Republic of Slovenia for awarding the nine months Mobility Grant (CMEPIUS) at the University of Ljubljana, Faculty of Chemistry and Chemical Technology. This article is also based upon work from COST Action EURESTOP, CA21145, supported by COST (European Cooperation in Science and Technology) and from Bilateral project No. 19 between University of Kragujevac, Faculty of Science, Serbia and University of Ljubljana, Faculty of Chemistry and Chemical Technology, Ljubljana, Slovenia. M. Z. acknowledges the support of the Science Fund of the Republic of Serbia for the computational part of this work (project #7750288, Tailoring Molecular Magnets and Catalysts Based on Transition Metal Complexes – TMMagCat).

References

- G. D. Brown, D. W. Denning, N. A. R. Gow, S. M. Levitz, M. G. Netea and T. C. White, *Sci. Transl. Med.*, 2012, **4**, 165rv13.
- K. C. Howard, E. K. Dennis, D. S. Watt and S. Garneau-Tsodikova, *Chem. Soc. Rev.*, 2020, **49**, 2426–2480.
- Y. Lin, H. Betts, S. Keller, K. Cariou and G. Gasser, *Chem. Soc. Rev.*, 2021, **50**, 10346–10402.
- J. Jampilek, *Expert Opin. Drug Discovery*, 2016, **11**, 1–9.
- M. A. Garcia-Solache and A. Casadevall, *mBio*, 2010, **18**, e00061–e00010.
- N. A. R. Gow, J.-P. Latge and C. A. Munro, *Microbiol. Spectrum*, 2017, **5**, DOI: [10.1128/microbiolspec.funk-0035-2016](https://doi.org/10.1128/microbiolspec.funk-0035-2016).
- D. J. Sheehan, C. A. Hitchcock and C. M. Sibley, *Clin. Microbiol. Rev.*, 1999, **12**, 40–79.
- G. Aperis and E. Mylonakis, *Expert Opin. Invest. Drugs*, 2006, **15**, 579–602.
- M. A. Pfaller, *Am. J. Med.*, 2012, **125**, S3–S13.
- M. A. Pfaller, D. J. Diekema, M. G. Rinaldi, R. Barnes, B. Hu, A. V. Veselov, N. Tiraboschi, E. Nagy, D. L. Gibbs and on behalf of the Global Antifungal Surveillance Group, *J. Clin. Microbiol.*, 2005, **43**, 5848–5859.
- S. Wu, Y. Wang, N. Liu, G. Dong and C. Sheng, *J. Med. Chem.*, 2017, **60**, 2193–2211.
- M. C. Fisher, N. J. Hawkins, D. Sanglard and S. J. Gurr, *Science*, 2018, **360**, 739–742.
- Y. Lee, E. Puumala, N. Robbins and L. E. Cowen, *Chem. Rev.*, 2021, **121**, 3390–3411.
- A. Frei, *Antibiotics*, 2020, **9**, 90.
- C. N. Morrison, K. E. Prosser, R. W. Stokes, A. Cordes, N. Metzler-Nolte and S. M. Cohen, *Chem. Sci.*, 2020, **11**, 1216–1225.
- A. W. Hung, A. Ramek, Y. Wang, T. Kaya, J. A. Wilson, P. A. Clemons and D. W. Young, *Proc. Natl. Acad. Sci. U. S. A.*, 2011, **108**, 6799–6804.
- W. H. B. Sauer and M. K. Schwarz, *J. Chem. Inf. Comput. Sci.*, 2003, **43**, 987–1003.
- W. R. J. D. Galloway, A. Isidro-Llobet and D. R. Spring, *Nat. Commun.*, 2010, **1**, 80.
- A. Frei, A. G. Elliott, A. Kan, H. Dinh, S. Bräse, A. E. Bruce, M. R. Bruce, F. Chen, D. Humaidy, N. Jung, A. P. King, P. G. Lye, H. K. Maliszewska, A. M. Mansour, D. Matiadis, M. Paz Muñoz, T.-Y. Pai, S. Pokhrel, P. J. Sadler, M. Sagnou, M. Taylor, J. J. Wilson, D. Woods, J. Zuegg, W. Meyer, A. K. Cain, M. A. Cooper and M. A. T. Blaskovich, *JACS Au*, 2022, **2**, 2277–2294.
- R. Navarro-Peñaloza, B. Landeros-Rivera, H. López-Sandoval, R. Castro-Ramírez and N. Barba-Behrens, *Coord. Chem. Rev.*, 2023, **494**, 215360.
- J. Kljun, A. J. Scott, T. Lanišnik Rižner, J. Keiser and I. Turel, *Organometallics*, 2014, **33**, 1594–1601.
- N. Lj. Stevanović, I. Aleksic, J. Kljun, S. Skaro Bogojevic, A. Veselinovic, J. Nikodinovic-Runic, I. Turel, M. I. Djuran and B. Đ. Glišić, *Pharmaceuticals*, 2021, **14**, 24.
- N. Lj. Stevanović, B. Đ. Glišić, S. Vojnovic, H. Wadepohl, T. P. Andrejević, S. Ž. Đurić, N. D. Savić, J. Nikodinovic-Runic, M. I. Djuran and A. Pavic, *J. Mol. Struct.*, 2021, **1232**, 130006.
- N. Lj. Stevanović, J. Kljun, I. Aleksic, S. Skaro Bogojevic, D. Milivojevic, A. Veselinovic, I. Turel, M. I. Djuran, J. Nikodinovic-Runic and B. Đ. Glišić, *Dalton Trans.*, 2022, **51**, 5322–5334.
- C. R. Groom, I. J. Bruno, M. P. Lightfoot and S. C. Ward, *Acta Crystallogr., Sect. B: Struct. Sci., Cryst. Eng. Mater.*, 2016, **72**, 171–179.
- Y. Cortat, M. Nedyalkova, K. Schindler, P. Kadakia, G. Demirci, S. Nasiri Sovari, A. Crochet, S. Salentinig, M. Lattuada, O. M. Steiner and F. Zobi, *Antibiotics*, 2023, **12**, 619.
- Y.-H. Ou, R.-K. Du, S.-P. Zhang, Y. Ling, S. Li, C.-J. Zhao, W.-Z. Zhang and L. Zhang, *J. Mol. Struct.*, 2020, **1215**, 128229.
- Q. Li, T. Wu, J.-C. Lai, Z.-L. Fan, W.-Q. Zhang, G.-F. Zhang, D. Cui and Z.-W. Gao, *Eur. J. Inorg. Chem.*, 2015, **2015**, 5281–5290.
- Q.-L. Ren, S.-S. Zhao, L.-X. Song, S.-S. Qian and J. Qin, *J. Coord. Chem.*, 2016, **69**, 227–237.
- N. D. Savić, S. Vojnovic, B. Đ. Glišić, A. Crochet, A. Pavic, G. V. Janjić, M. Pekmezović, I. M. Opsenica, K. M. Fromm, J. Nikodinovic-Runic and M. I. Djuran, *Eur. J. Med. Chem.*, 2018, **156**, 760–773.
- A. B. D. Nandiyanto, R. Oktiani and R. Ragadhita, *Indones. J. Sci. Technol.*, 2019, **4**, 97–118.
- J.-A. Zhang, M. Pan, J.-Y. Zhang, H.-K. Zhang, Z.-J. Fan, B.-S. Kang and C.-Y. Su, *Polyhedron*, 2009, **28**, 145–149.
- Y. Jiang, C.-F. Zhu, Z. Zheng, J.-B. He and Y. Wang, *Inorg. Chim. Acta*, 2016, **451**, 143–147.
- S. Medici, M. Peana, V. M. Nurchi and M. A. Zoroddu, *J. Med. Chem.*, 2019, **62**, 5923–5943.
- J. Kujawski, K. Czaja, E. Jodłowska, K. Dettlaff, M. Politańska, J. Żwawiak, R. Kujawski, T. Ratajczak, M. K. Chmielewski and M. K. Bernard, *J. Mol. Struct.*, 2016, **1119**, 250–258.



- 36 W. Liu, K. Bendorf, A. Hagenbach, U. Abram, B. Niu, A. Mariappan and R. Gust, *Eur. J. Med. Chem.*, 2011, **46**, 5927–5934.
- 37 U. Kalinowska-Lis, A. Felczak, L. Chęcińska, M. Małecka, K. Lisowska and J. Ochocki, *New J. Chem.*, 2016, **40**, 694–704.
- 38 N. Stevanović, M. Zlatar, I. Novaković, A. Pevec, D. Radanović, I. Z. Matic, M. Đorđić Crnogorac, T. Stanojković, M. Vujčić, M. Gruden, D. Sladić, K. Anđelković, I. Turel and B. Čobeljić, *Dalton Trans.*, 2021, **51**, 185–196.
- 39 T. P. Andrejević, I. Aleksic, J. Kljun, M. Počkaj, M. Zlatar, S. Vojnovic, J. Nikodinovic-Runic, I. Turel, M. I. Djuran and B. Glišić, *RSC Adv.*, 2023, **13**, 4376–4393.
- 40 M. Baranowska, K. Suliborska, W. Chrzanowski, B. Kusznierevich, J. Namieśnik and A. Bartoszek, *Redox Biol.*, 2018, **17**, 355–366.
- 41 T. P. Andrejević, D. Milivojevic, B. Đ. Glišić, J. Kljun, N. Lj. Stevanović, S. Vojnovic, S. Medic, J. Nikodinovic-Runic, I. Turel and M. I. Djuran, *Dalton Trans.*, 2020, **49**, 6084–6096.
- 42 J.-Y. Wu, Y.-L. Pan, X.-J. Zhang, T. Sun, Y.-P. Tian, J.-X. Yang and Z.-N. Chen, *Inorg. Chim. Acta*, 2007, **360**, 2083–2091.
- 43 P. Połczyński, R. Jurczakowski and W. Grochala, *J. Phys. Chem. C*, 2013, **117**, 20689–20696.
- 44 K. D. Trotter, O. Owajaye, S. P. Meredith, P. E. Keating, M. D. Spicer, J. Reglinski and C. M. Spickett, *BioMetals*, 2019, **32**, 627–640.
- 45 J. H. B. Nunes, D. H. Nakahata, P. P. Corbi and R. E. F. de Paiva, *Coord. Chem. Rev.*, 2023, **490**, 215228.
- 46 T. Bruna, F. Maldonado-Bravo, P. Jara and N. Caro, *Int. J. Mol. Sci.*, 2021, **22**, 7202.
- 47 D. Żyro, L. Radko, A. Śliwińska, L. Chęcińska, J. Kusz, I. Korona-Główniak, A. Przekora, M. Wójcik, A. Pośniak and J. Ochocki, *Cancers*, 2022, **14**, 900.
- 48 N. A. Johnson, M. R. Southerland and W. J. Youngs, *Molecules*, 2017, **28**, 1263.
- 49 S. Medici, M. Peana, V. M. Nurchi, J. I. Lachowicz, G. Crisponi and M. A. Zoroddu, *Coord. Chem. Rev.*, 2015, **284**, 329–350.
- 50 S. Medici, M. Peana, G. Crisponi, V. M. Nurchi, J. I. Lachowicz, M. Remelli and M. A. Zoroddu, *Coord. Chem. Rev.*, 2016, **327–328**, 349–359.
- 51 N. D. Savić, B. B. Petković, S. Vojnovic, M. Mojicevic, H. Wadepohl, K. Olaiya, E. Marsili, J. Nikodinovic-Runic, M. I. Djuran and B. Đ. Glišić, *Dalton Trans.*, 2020, **49**, 10880–10894.
- 52 A. G. Warrilow, J. E. Parker, D. E. Kelly and S. L. Kelly, *Antimicrob. Agents Chemother.*, 2013, **57**, 1352–1360.
- 53 J. A. Romo, C. G. Pierce, A. K. Chaturvedi, A. L. Lazzell, S. F. McHardy, S. P. Saville and J. L. Lopez-Ribot, *mBio*, 2017, **8**, e01991–e01917.
- 54 T. P. Andrejević, I. Aleksic, J. Kljun, M. Počkaj, M. Zlatar, S. Vojnovic, J. Nikodinovic-Runic, I. Turel, M. I. Djuran and B. Đ. Glišić, *RSC Adv.*, 2023, **13**, 4376–4393.
- 55 H. T. Taff, K. F. Mitchell, J. A. Edward and D. R. Andes, *Future Microbiol.*, 2013, **8**, 1325.
- 56 F. Saleh, A. Harb, N. Soudani and H. Zaraket, *J. Infect. Public Health*, 2020, **13**, 1142–1147.
- 57 A. J. Carterson, K. Höner zu Bentrup, C. M. Ott, M. S. Clarke, D. L. Pierson, C. R. Vanderburg, K. L. Buchanan, C. A. Nickerson and M. J. Schurr, *Infect. Immun.*, 2005, **73**, 1129–1140.
- 58 K. S. dos Santos, L. T. Oliveira, M. de Lima Fontes, K. F. Migliato, A. M. Fusco-Almeida, M. J. S. M. Giannini and A. Moroz, *J. Fungi*, 2023, **9**, 634.
- 59 K. E. de Visser, A. Eichten and L. M. Coussens, *Nat. Rev. Cancer*, 2006, **6**, 24–37.
- 60 J. Kljun, I. E. Leon, Š. Peršič, J. F. Cadavid-Vargas, S. B. Etcheverry, W. He, Y. Bai and I. Turel, *J. Inorg. Biochem.*, 2018, **186**, 187.
- 61 *Crysalis PRO*, Oxford Diffraction Ltd, Yarnton, Oxfordshire, England, 2011.
- 62 O. V. Dolomanov, L. J. Bourhis, R. J. Gildea, J. A. K. Howard and H. Puschmann, *J. Appl. Crystallogr.*, 2009, **42**, 339–341.
- 63 G. M. Sheldrick, *Shelxl 2018/3*, University of Göttingen, Germany, 2018.
- 64 C. F. Macrae, P. R. Edgington, P. McCabe, E. Pidcock, G. P. Shields, R. Taylor, M. Towler and J. Van De Streek, *J. Appl. Crystallogr.*, 2006, **39**, 453–457.
- 65 G. te Velde, F. M. Bickelhaupt, E. J. Baerends, C. Fonseca Guerra, S. J. A. van Gisbergen, J. G. Snijders and T. Ziegler, *J. Comput. Chem.*, 2001, **22**, 931–967.
- 66 R. Rüger, M. Franchini, T. Trnka, A. Yakovlev, E. van Lenthe, P. Philipsen, T. van Vuren, B. Klumpers and T. Soini, AMS 2023.1, SCM, Theoretical Chemistry, Vrije Universiteit, Amsterdam, The Netherlands, <https://www.scm.com>.
- 67 E. van Lenthe, E. J. Baerends and J. G. Snijders, *J. Chem. Phys.*, 1993, **99**, 4597–4610.
- 68 E. van Lenthe, E. J. Baerends and J. G. Snijders, *J. Chem. Phys.*, 1994, **101**, 9783–9792.
- 69 C. van Wüllen, *J. Chem. Phys.*, 1998, **109**, 392–399.
- 70 A. Klamt and G. Schoermann, *J. Chem. Soc., Perkin Trans. 2*, 1993, 799–805.
- 71 A. Klamt, *J. Phys. Chem.*, 1995, **99**, 2224–2235.
- 72 C. C. Pye and T. Ziegler, *Theor. Chem. Acc.*, 1999, **101**, 396–408.
- 73 A. D. Becke, *Phys. Rev. A*, 1988, **38**, 3098–3100.
- 74 J. P. Perdew, *Phys. Rev. B: Condens. Matter Mater. Phys.*, 1986, **33**, 8822–8824.
- 75 J. P. Perdew, *Phys. Rev. B: Condens. Matter Mater. Phys.*, 1986, **34**, 7406–7406.
- 76 E. Caldeweyher, S. Ehlert, A. Hansen, H. Neugebauer, S. Spicher, C. Bannwarth and S. Grimme, *J. Chem. Phys.*, 2019, **150**, 154122.
- 77 Y. P. Li, J. Gomes, S. M. Sharada, A. T. Bell and M. Head-Gordon, *J. Phys. Chem. C*, 2015, **119**, 1840–1850.
- 78 S. Grimme, *Chem. – Eur. J.*, 2012, **18**, 9955–9964.
- 79 H. S. Yu, X. He, S. L. Li and D. G. Truhlar, *Chem. Sci.*, 2016, **7**, 5032–5051.
- 80 J. Tao, J. Perdew, V. Staroverov and G. Scuseria, *Phys. Rev. Lett.*, 2003, **91**, 146401.



- 81 V. N. Staroverov, G. E. Scuseria, J. Tao and J. P. Perdew, *J. Chem. Phys.*, 2003, **119**, 12129.
- 82 S. Lehtola, C. Steigemann, M. J. T. Oliveira and M. A. L. Marques, *SoftwareX*, 2018, **7**, 1–5.
- 83 M. C. Arendrup, M. Cuenca-Estrella, C. Lass-Flörl and W. Hope, EUCAST-AFST, *Clin. Microbiol. Infect.*, 2012, **18**, E246–E247.
- 84 T. Mosmann, *J. Immunol. Methods*, 1983, **65**, 55–63.
- 85 B. A. Arthington-Skaggs, H. Jradi, T. Desai and C. J. Morrison, *J. Clin. Microbiol.*, 1999, **39**, 3332–3337.
- 86 H. Liu, J. Köhler and G. R. Fink, *Science*, 1994, **266**, 1723–1726.
- 87 C. G. Pierce, P. Uppuluri, A. R. Tristan, F. L. Wormley Jr., E. Mowat, G. Ramage and J. L. Lopez-Ribot, *Nat. Protoc.*, 2008, **3**, 1494–1500.
- 88 A. Jakab, S. Mogavero, T. M. Forster, M. Pekmezovic, N. Jablonowski, V. Dombradi, I. Pocsi and B. Hube, *Microbiology*, 2016, **162**, 2116–2125.
- 89 B. Wächtler, D. Wilson, K. Haedicke, F. Dalle and B. Hube, *PLoS One*, 2011, **6**, e17046.

